Article

The Impact of Graphene Oxide on Polycaprolactone PCL Surfaces: Antimicrobial Activity and Osteogenic Differentiation of Mesenchymal Stem Cell

Letizia Ferroni [1], Chiara Gardin [1], Federica Rigoni [2], Eleonora Balliana [3], Federica Zanotti [4], Marco Scatto [2,5], Pietro Riello [2] and Barbara Zavan [4,*]

1 Maria Cecilia Hospital, GVM Care & Research, 48033 Cotignola, Ravenna , Italy; lferroni@gvmnet.it (L.F.); gardinc@gvmnet.it (C.G.)
2 Department of Molecular Sciences and Nanosystems, Ca' Foscari University of Venice, Via Torino 155, 30172 Venezia Mestre, Venice, Italy; rigonii@unive.it (F.R.); scattom@gmail.it (M.S.); riellop@unive.it (P.R.)
3 Department of Environmental Sciences and Statistics, Ca' Foscari University of Venice, Via Torino 155, 30172 Venezia Mestre, Venice, Italy; eballiana@unive.it
4 Department of Translational Medicine, University of Ferrara, Via Fossato di Mortara 70, 44121 Ferrara, Ferrara, Italy; zanottiff@unife.it
5 Nadir S.r.l., Via Torino 155b, c/o Department of Molecular Sciences and Nanosystems, Ca' Foscari University of Venice, Via Torino 155, 30172 Venezia Mestre, Venice, Italy
* Correspondence: barbara.zavan@unife.it

Abstract: In dentistry, bone regeneration requires osteoinductive biomaterial with antibacterial properties. Polycaprolactone (PCL) may be combined with different nanofillers including reduced graphene oxide (rGO). Here, the amount of rGO filler was defined to obtain a biocompatible and antibacterial PCL-based surface supporting the adhesion and differentiation of human mesenchymal stem cells (MSCs). Compounds carrying three different percentages of rGO were tested. Among all, the 5% rGO-PCL compound is the most bacteriostatic against Gram-positive bacteria. All scaffolds are biocompatible. MSCs adhere and proliferate on all scaffolds; however, 5% rGO-PCL surface supports the growth of cells and implements the expression of extracellular matrix components necessary to anchor the cells to the surface itself. Moreover, the 5% rGO-PCL surface has superior osteoinductive properties confirmed by the improved alkaline phosphatase activity, mineral matrix deposition, and osteogenic markers expression. These results suggest that 5% rGO-PCL has useful properties for bone tissue engineering purposes.

Keywords: graphene; polycaprolactone; antimicrobial surfaces; mesenchymal stem cell; adhesion; differentiation; bone

1. Introduction

In dentistry, bone regeneration is crucial in cases of trauma, infections, and tumors, and it is sometimes required to stabilize dental implants [1]. De facto, implant therapy is effective when an adequate vertical and horizontal bone volume is present at the implant site [2]. Bone augmentation usually requires bone blocks or granulated bone particulates and membrane or titanium meshwork. This can be technically challenging, and the success of the treatment will depend on the space maintenance of the regenerated defect, wound stability, and absence of infection [3]. When bacterial activity occurs in bone defects, bone regeneration can be limited or even hindered. For this reason, novel biomaterials for bone regeneration are still extensively investigated. Currently, most commercial biomaterials are slightly osteoinductive and with poor antibacterial properties [1].

Polycaprolactone (PCL) is a biocompatible, semicrystalline, water-insoluble polymer, which has gained much attention in scaffolding and tissue engineering due to its adaptability and tailorable properties [4]. Thanks to its good ability of plasticity under a certain

stress without fracturing, PCL represents a perfect chosen material in dental and orthopedic regenerative medicine [5,6]. In addition, PCL can be combined with a low concentration of specific nanomaterials for the fabrication of scaffolds with definite features for cell and tissue growth. The mechanical properties of nanocomposite polymers depend on the properties of both pure polymer and filler [7]. In recent years, a large body of investigation has been dealing with nanofiller as a reinforcement to improve or introduce new properties at the nano- and macro-scale. Graphene-related materials, including graphene oxide (GO), reduced graphene oxide (rGO), or graphene nanoplates, were embedded in PCL to enhance the crystallization and orientation of polymer matrix or to make PCL conductive [8–10].

Nowadays, stem cells are offering revolutionary therapies for many diseases with limited treatment options. They play a crucial role in tissue repair, as they possess the unique quality to differentiate into specialized cell types in response to biochemical, biophysical, and biomechanical cues. In fact, stem cells adapt themselves to the surrounding environment and to the specific features of the scaffold, including composition, surface topography, ligand availability, and mechanical properties changing migration, proliferation, differentiation, and viability [11,12].

In this work, PCL/rGO composites have been investigated for regenerative medicine purposes as substrates for stem cell proliferation and differentiation. Pure PCL was mixed with three different percentage of rGO (1.6%, 3%, and 5%) to manufacture by extrusion rGO-PCL compounds. First chemical composition, antibacterial activity, and biocompatibility of rGO-PCL compounds were screened. Second, the regenerative properties of the composites were investigated in vitro with human mesenchymal stem cells (HMSCs). All compounds were biocompatible in conformity with the international standard for medical devices and bacteriostatic to Gram-positive bacteria in rGO-dose dependent manner. The percentage of rGO also regulated the adhesion, morphology, and differentiation of the stem cells. rGO impacted the osteogenic differentiation by ensuring the activity of alkaline phosphatase, the deposition of the mineral matrix, and the expression of proteins crucial for the differentiation in osteoblasts. These results suggest that 5% rGO-PCL has useful properties for bone tissue engineering purposes.

2. Materials and Methods

2.1. Compounds Preparation

Pure PCL (Sigma-Aldrich, St. Louis, MO, USA) was mixed with rGO (Abalonyx AS, Oslo, Norway) at the percentages of 1.6% *w/w*, 3% *w/w,* or 5% *w/w* through melt compounding strategy assisted by a twin screw extruder (Themo Fisher Scientific, Waltham, MA, USA) by Nadir s.r.l. PCL pellets were placed in the extruder's pellet feeder, whereas the rGO were placed in the extruder's filler feeder. Next, during the extrusion process, all the materials were fed at the same time to produce a compounded wire that was immediately ground to form composite pellets. After drying the composite pellets at 50 °C, injection molding was performed to manufacture disks. All samples were sterilized with ethylene oxide.

2.2. Chemical Characterization

Raman spectra were recovered using a dispersive Raman system Thermo Scientific™ DXR3™ (Waltham, MA, USA) equipped with an Olympus microscope. The experimental parameters were laser wavelengths 532 nm, power laser of 5 mW, and 50–3350 cm^{-1} full range grating. A 10× objective and a 25 μm-slit aperture were used to obtain more representative spectra from the samples. Total acquisition time for each spectrum was 120 s. Thermo Scientific™ OMNIC™ software 34.3 (Version 3, Waltham, MA, USA) was used to operate the DXR3™ Raman Microscope and to collect the spectra. Raman spectra were compared with the internal library of instrument and with literature for peak assignment.

2.3. Antibacterial Activity

Antibacterial activity of rGO-PCL compounds was evaluated against Streptococcus pyogenes, Staphylococcus aureus, Escherichia coli, and Pseudomonas aeruginosa (all purchased from ATCC, Manassas, VA, USA). Antibacterial assays were performed according to ISO 22196:2011 (Measurement of antibacterial activity on plastics and other non-porous surfaces). The agar diffusion method and the quantification of colony forming units (CFU) were performed. *P. aeruginosa* virulence was evaluated by quantification of pyocyanin production. *E. coli* adhesion was monitored by fluorescent miscopy. A suspension of recombinant *E. coli* bacteria expressing green fluorescent protein GFP (E. coli-GFP; ATCC) was placed in contact with samples at 37 °C with shaking for 24 h and then observed at microscope.

2.4. In Vitro Cytotoxicity

The in vitro cytotoxicity of rGO-PCL compounds was evaluated following the ISO 10993-5 standard test method (Biological evaluation of medical devices—Part 5: Tests for in vitro cytotoxicity) [13]. Briefly, NCTC clone 929 (mouse fibroblast cell line; ATCC) were seeded at the density of 2×10^4 cell/cm^2 in Dulbecco's Modified Eagle Medium (DMEM, EuroClone, Rome, Italy) supplemented with 10% Fetal Bovine Serum (FBS, EuroClone) and 1% Penicillin-Streptomycin (PS, EuroClone). After 24 h, rGO-PCL compounds were placed in direct contact with cells for 48 h. Then, cell viability was determined by incubation with 0.5 mg/mL MTT (Sigma-Aldrich) solution for 3 h. After removing the MTT solution, extraction solution (isopropanol:dimethyl sulfoxide 9:1) was incubated for 30 min at 37 °C, and absorbance at 570 nm was recorded. NCTC in direct contact with sterile titanium was used as control condition. Results were expressed as the percentage of viable cells [14].

2.5. Stem Cell Seeding on rGO-PCL Surfaces

rGO-PCL disks were positioned on the bottom of 24-well plates and 2×10^4 human Adipose-derived Mesenchymal Stem Cells (HMSCs, Sciencell Research Laboratories, New York, NY, USA) were seeded on each of them. Cultures have been maintained in osteogenic differentiation medium consisting in DMEM supplemented with 10% FBS, 1% PS, 10 ng/mL Fibroblast Growth Factor 2 (FGF-2, ProSpec, New York, NY, USA), 10 mM β-glycerophosphate (Sigma-Aldrich, St. Louis, MO, USA), and 10 nM dexamethasone (Sigma-Aldrich, St. Louis, MO, USA). All cultures were incubated at 37 °C and 5% CO$_2$ for up to 21 days, and culture medium was changed three times a week [15]. These cultures were investigated for cell adhesion, mechanical properties, morphology, cell viability, alkaline phosphatase (ALP) activity, mineral matrix deposition, and gene expression.

2.6. Cell Adhesion, Morphology, and Proliferation

The adhesion and morphology of HMSCs on rGO-PCL surfaces were evaluated using the ZEISS SIGMA VP Field Emission Scanning Electron Microscope (FE-SEM, ZEISS, Jena, Germany). Samples were fixed with 2% glutaraldehyde (Sigma-Aldrich, St. Louis, MO, USA) in 0.1 M HEPES buffer (Sigma-Aldrich, St. Louis, MO, USA), dehydrated in ethanol, and chemical dried with hexamethyldisilane (Sigma-Aldrich, St. Louis, MO, USA) [16]. The SEM images of the sample surfaces were recorded in high vacuum (10^{-6} mbar) after the surface metallization with a gold thin film by using a Polaron SC7620 gold sputter coater.

MTS Assay (Abcam, Cambridge, UK) quantified the viability and proliferation of HMSCs on each surface. Briefly, cells were incubated with MTS compound for 4 h at 37 °C and 5% CO$_2$. Then, the produced formazan was quantified by measuring the absorbance at 490 nm.

2.7. ALP Activity

ALP activity was detected by Alkaline phosphates kit (Abcam) that uses p-nitrophenyl phosphate (pNPP) as phosphatase substrate and adsorbed at 405 nm when dephosphory-lated by ALP. According to the manufacturer protocol, cells were lysed with ALP Assay

Buffer [17]. Samples were incubated with pNPP for 60 min at 25 °C, and then the absorbance at 405 nm was measured. ALP activity in test samples was calculated as follows:

$$\text{ALP activity (U/L)} = (B/\Delta T \times V) \times D \times 1000 \tag{1}$$

where B is the amount of pNP in sample well calculated from standard curve (μmol), ΔT is the reaction time (minutes), V is the original sample volume added into the reaction well (mL), D is the sample dilution factor [18].

2.8. Quantification of Mineral Matrix Deposition

The deposit of mineral matrix was evaluated by Alizarin Red S (ARS) quantification. After fixation with 10% formalin (Sigma), the staining with 40 mM ARS solution (Sigma-Aldrich) was performed for 20 min with gentle shaking. After washing with ddH2O, ARS staining was extracted with 0.5 mL of 10% acid acetic solution for 20 min with gentle agitation. The extracts were measured at 570 nm in a plate reader (Victor 3 Perkin Elmer).

2.9. Gene Expression Profile

Total RNA was extracted with Total RNA Purification Plus Kit (Norgen Biotek Corporation, Thorold, ON, Canada), according to the manufacture procedures. The RT2 Profiler PCR Array Human Extracellular Matrix and Adhesion Molecules (Qiagen, Hilden, Germany) were performed by reverse transcribing 200 ng of total RNA, following the manufacture procedures. The Ct values of target genes were normalized to the geometric mean Ct values of five housekeeping genes (ACTB: actin, beta; B2M: beta-2-microglobulin; GAPDH: glyceraldehyde-3-phosphate dehydrogenase; HPRT1: hypoxanthine phosphoribosyltransferase 1; RPLP0: ribosomal protein, large, P0). The expression of osteogenesis-related genes including osteocalcin (OC), osteopontin (OPN), runt-related transcription factor 2 (RUNX2), osterix (OSX), receptor activator of NF-kB ligand (RANKL), and alpha-1 type I collagen (COL1A1) was investigated at day 7, 14, and 21. Total RNA was reverse transcribed with SensiFAST cDNA Synthesis kit (Bioline GmbH, Luckenwalde, Germany) following the manufacture conditions. Real-time PCR was performed using SensiFAST SYBR No-ROX mix (Bioline GmbH) with 400 nM primers (selected by Primer 3 software3, Bioline, NY, USA). Ct values of target genes were normalized to the geometric mean Ct values of two housekeeping genes (B2M; GAPDH). Data analysis was performed using the 2ΔΔCt method [18]. Results were reported as fold change of target genes on rGO/PCL composites compared with PCL (control).

2.10. Statistical Analysis

All data were expressed as mean and standard deviation (mean ± SD), one-way analysis of variance (ANOVA), and two-tailed *t*-test were utilized to assess the statistical significance with p-value < 0.05.

3. Results

3.1. Chemical Characterization of rGO-PCL Compounds

The different rGO-PCL compounds were manufactured through the dispersion of low percentage of rGO in order to do not change the bulk macroscopic properties of the substrate such as mechanical and rheological properties. Three percentages of rGO powder (1.6% *w/w*, 3% *w/w* or 5% *w/w*) were well dispersed into melted PCL using a lab-scale twin-screw extruder at temperatures ranging between 55 and 60 °C. Raman spectra of rGO-PCL compounds were compared to pure PCL and pure rGO (Figure 1). The spectrum of pure PCL (Figure 1a) is characterized by two intense bands for CH_2 antisymmetric and symmetric stretching at 2870 cm^{-1} and 2920 cm^{-1}, respectively. The bands at 1728 cm^{-1} (νC=O), at 1110 cm^{-1} (νCOC), and at about 1728 cm^{-1} reflect the crystalline domains of PCL. The other narrow peaks at 916 cm^{-1} (νC–COO), between the spectral range 1046–1110 cm^{-1} (νCOC), and 1298–1419 cm^{-1} (δCH2) are also related to PCL crystalline nature. The remaining minor peaks, such as the broad band at about 860 cm^{-1}, are

attributable to the amorphous part of PCL, here present mainly as residues [19–21]. Raman spectrum of pure rGO (Figure 1e) is characterized by two main bands at ~1350 cm^{-1} and at ~1593 cm^{-1} associated to the well-known D-band and the G-band, respectively [22,23]. In 1.6% rGO-PCL (Figure 1b), 3% rGO-PCL (Figure 1c), and 5% rGO-PCL (Figure 1d) the D- and G-band are also present. In particular, 1.6% rGO-PCL sample presents the peculiar peaks and bands of both PCL and rGO. Whereas in 3% rGO-PCL and 5% rGO-PCL samples the D- and G-band are the dominant features due to the cover effect of rGO on PCL film. However, although less intense, the PCL CH$_2$ related bands at 2870 cm^{-1} and 2920 cm^{-1} are also detectable.
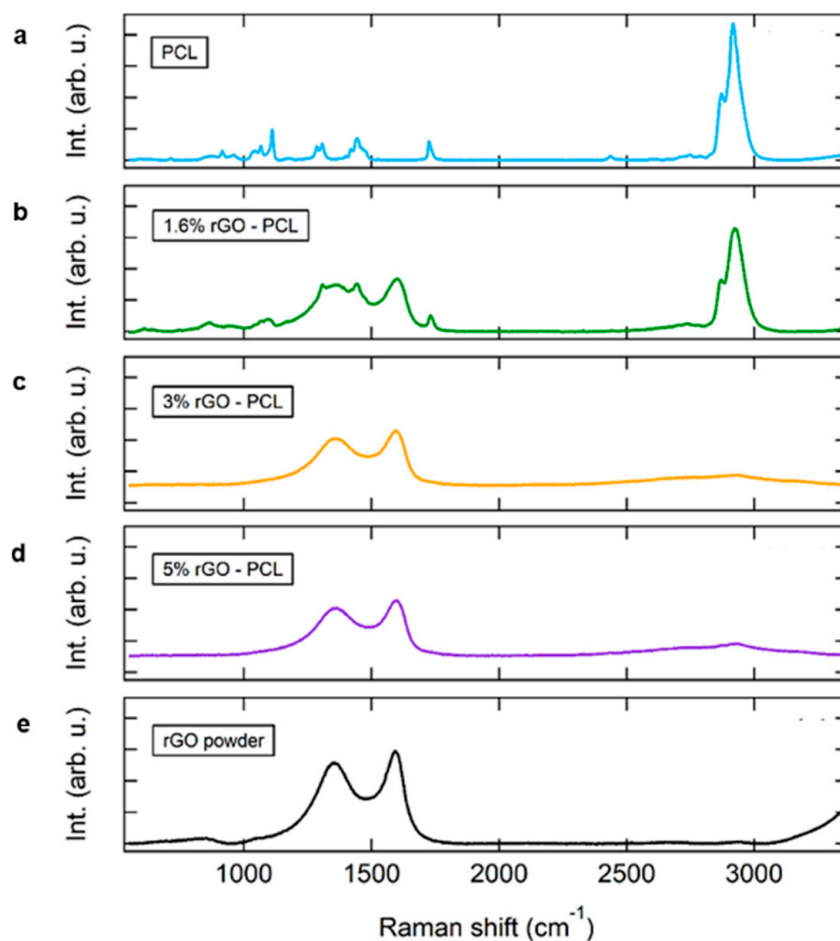
Figure 1. Raman spectra: PCL (**a**), 1.6% rGO-PCL (**b**), 3% rGO-PCL (**c**), 5% rGO-PCL (**d**), and rGO powder (**e**).

3.2. Antibacterial Activity and Cytotoxicity Evaluation of rGO-PCL Compounds

The antibacterial property of each rGO-PCL compound was investigated by means of different approaches, including the agar diffusion method, the count of CFU after treatment or seeding with Gram-positive (*S. pyogenes* and *S. aureus*) or Gram-negative (*E. coli* and *P. aeruginosa*) bacteria, the production of pyocyanin, and the adhesion of E. coli-GFP.

For agar diffusion method, samples were placed in Mueller–Hinton plates seeded with *S. pyogenes*, *S. aureus*, *E. coli*, or *P. aeruginosa*. After 24 h, the inhibition zone around the samples were evaluated. Inhibition zones (diameter 1 mm) were present around 1.6% rGO-PCL, 3% rGO-PCL, and 5% rGO-PCL in *S. aureus* cultures. In case of *S. pyogenes* culture, inhibition region of 1 mm was observed around 1.6% rGO-PCL and 3% rGO-PCL, and inhibition zone of 2 mm around 5% rGO-PCL. Suspensions of each bacterium were incubated with the samples for 1, 4, and 24 h in order to quantify the CFU of bacteria after 24 h of incubation (Table 1). *E. coli* and *P. aeruginosa* growth was not affected by any

tested sample. Concentrations of 1.6% rGO-PCL and 3% rGO-PCL have slight bacteriostatic effect against *S. aureus* after 24 h of contact, whereas the increase in contact time yielded an increased bacteriostatic action for 5% rGO-PCL against *S. aureus*. The *S. pyogenes* growth is slightly affected by 5% rGO-PCL after 24 h of treatment. Moreover, the proliferation of 100 bacteria was evaluated after the direct seeding on the samples for 1, 3, and 24 h, and subsequently buffered on a plate (Table 2). Among tested samples, 5% rGO-PCL have bacteriostatic activity on *E. coli*, *S. aureus*, and *S. pyogenes*. The effect of the samples against Gram-negative bacteria was also detected by monitoring the adhesion of *E. coli*, and the production of pyocyanin in *P. aeruginosa*. The *E. coli* adhesion was greater on 1.6% rGO-PCL than on 3% rGO-PCL and 5% rGO-PCL. Instead, the production of pyocyanin in *P. aeruginosa* has been reduced by 27.7% for 1.6% rGO-PCL, 23.34% for 3% rGO-PCL, and 17.58% for 5% rGO-PCL.

Table 1. Colony forming units (CFU) of *E. coli*, *P. aeruginosa*, *S. aureus*, and *S. pyogenes* after treatment with 1.6% rGO-PCL, 3% rGO-PCL, and 5% rGO-PCL for 1, 4, and 24 h.

|	Log (CFU/cm^2)			
Time	1.6% rGO-PCL	3% rGO-PCL	5% rGO-PCL	Control
	E. coli			
1 h	1.30 (r = −0.02)	1.38 (r = −0.1)	1.23 (r = 0.05)	1.28
4 h	1.76 (r = −0.03)	1.80 (r = −0.07)	1.69 (r = 0.04)	1.73
24 h	2.20 (r = −0.1)	2.20 (r = −0.1)	2.05 (r = 0.05)	2.10
	P. aeruginosa			
1 h	1.58 (r = −0.54)	1.38 (r = −0.34)	1.41 (r = −0.37)	1.04
4 h	1.96 (r = −0.38)	1.82 (r = −0.24)	1.85 (r = −0.27)	1.58
24 h	2.19 (r = 0.01)	2.21 (r = −0.01)	2.23 (r = −0.03)	2.20
	S. aureus			
1 h	1.34 (r = −0.08)	1.38 (r = −0.12)	0.95 (r = 0.31)	1.26
4 h	1.69 (r = −0.11)	1.70 (r = −0.12)	1.23 (r = 0.35)	1.58
24 h	1.90 (r = 0.33)	1.98 (r = 0.25)	1.62 (r = 0.61)	2.23
	S. pyogenes			
1 h	0.84 (r = 0.0)	0.9 (r = −0.06)	0.78 (r = 0.06)	0.84
4 h	1.15 (r = −0.04)	1.18 (r = −0.07)	1.11 (r = 0.0)	1.11
24 h	1.41 (r = 0.07)	1.5 (r = −0.02)	1.34 (r = 0.14)	1.48

r: correlation coefficient.

Table 2. Colony forming units (CFU) of *E. coli*, *P. aeruginosa*, *S. aureus*, and *S. pyogenes* after seeding on 1.6% rGO-PCL, 3% rGO-PCL, and 5% rGO-PCL for 1, 4, and 24 h.

|	Log (CFU/cm^2)			
Time	1.6% rGO-PCL	3% rGO-PCL	5% rGO-PCL	Control
	E. coli			
1 h	1.18 (r = 0.0)	1.15 (r = 0.03)	1.00 (r = 0.18)	1.18
4 h	1.54 (r = −0.01)	1.50 (r = 0.03)	1.40 (r = 0.13)	1.53
24 h	2.04 (r = 0.0)	2.02 (r = 0.05)	1.91 (r = 0.15)	2.04
	P. aeruginosa			
1 h	1.15 (r = −0.07)	1.08 (r = 0.0)	1.11 (r = −0.03)	1.08
4 h	1.59 (r = −0.02)	1.59 (r = −0.02)	1.56 (r = 0.01)	1.57
24 h	2.18 (r = −0.01)	2.21 (r = −0.04)	2.19 (r = −0.02)	2.17
	S. aureus			
1 h	1.34 (r = 0.0)	1.30 (r = 0.04)	0.95 (r = 0.39)	1.34
4 h	1.62 (r = 0.04)	1.61 (r = 0.05)	1.28 (r = 0.38)	1.66
24 h	1.87 (r = 0.21)	1.99 (r = 0.09)	1.83 (r = 0.25)	2.08
	S. pyogenes			
1 h	1.00 (r = 0.08)	0.9 (r = 0.18)	0.78 (r = 0.30)	1.08
4 h	1.15 (r = 0.13)	1.18 (r = 0.10)	1.08 (r = 0.20)	1.28
24 h	1.36 (r = 0.05)	1.38 (r = 0.03)	1.30 (r = 0.11)	1.41

r: correlation coefficient.

The biocompatibility of rGO-PCL was assessed by measuring the viability of murine fibroblasts (NCTC clone 929) according to the International Organization for Standardization (ISO 10993-5) that assess the in vitro cytotoxicity of medical devices. The viability of the fibroblasts incubated with rGO-PCL compounds ranged between ~81 and ~90% (Figure 2). According to ISO 10993-5, a reduction in cell viability by more than 30% is considered a cytotoxic effect. Therefore, all rGO-PCL compounds exhibited no toxicity against NCTC clone 929 cells.
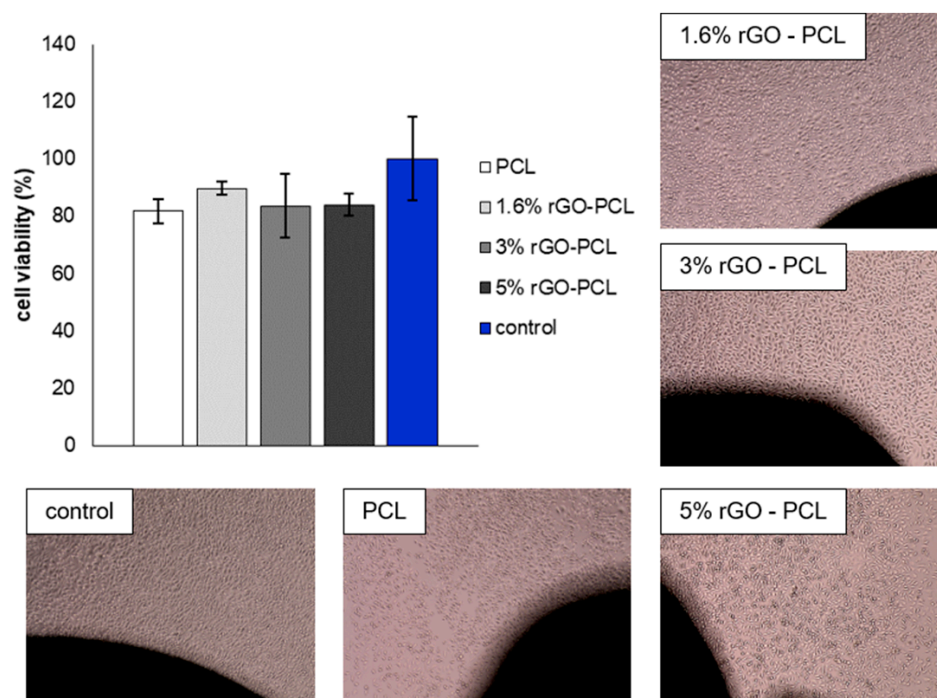
Figure 2. In vitro cytotoxicity evaluation of rGO-PCL compounds. Cell viability percentage of murine fibroblasts (NCTC clone 929) in contact with rGO-PCL compounds for 48 h. Sterile titanium was used as control. Data are expressed as mean $\pm$ SD. Multi comparison statistical analyses were performed by using one-way ANOVA. A T test was performed for all pairwise comparisons between group means. Representative images show fibroblasts after 48 h of culture with each sample.

3.3. Stem Cells Adhesion on rGO-PCL Surfaces

HMSCs were seeded and maintained on each rGO-PCL surface for 7 days. In general, the cells have adhered and migrated over the substrates, as shown by the representative SEM images in Figure 3a–d. The cells on rGO-PCL surfaces appeared flat (Figure 3b–d); on the contrary, on pure PCL cells were fusiform (Figure 3a). The gene expression of molecules and proteins of extracellular matrix (ECM) was investigated by real time PCR array (Figure 3e). On rGO-PCL, with more extension on the 5% rGO-PCL surface, the mRNA encoding CD44, COL4A2, CTNNA1, CTNNB1, ECM1, ITGA2, ITGA4, LAMA1, MMP11, SGCE, and TIMP1 genes were upregulated, whereas ITGAM, ITGA1, LAMB3, and VCAM1 were under-expressed genes.
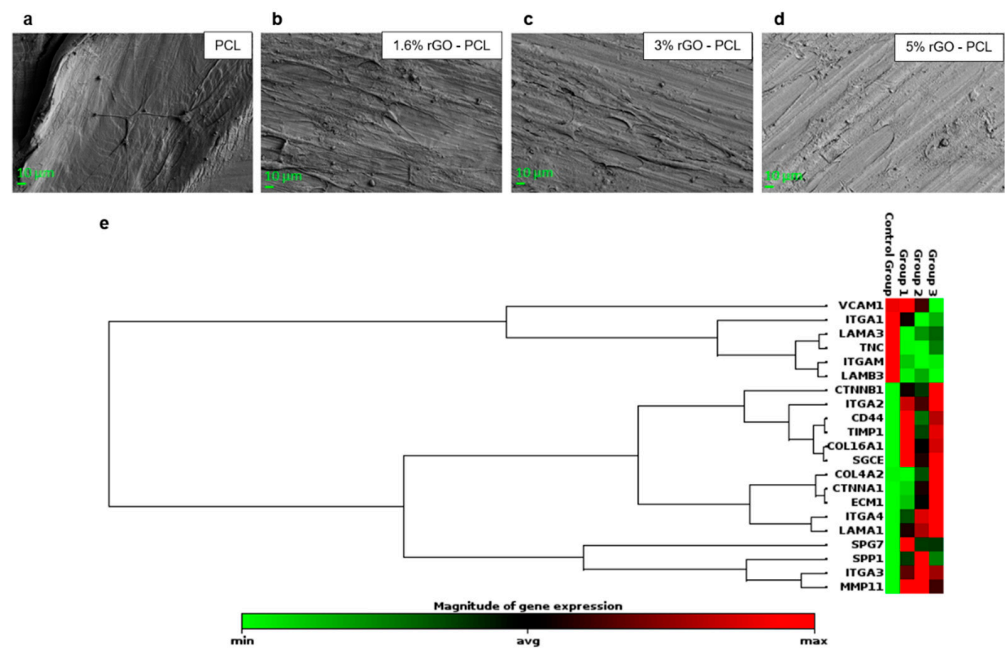
Figure 3. Stem cells adhesion on rGO-PCL surfaces. SEM images of the cells on pure PCL (**a**), 1.6% rGO-PCL (**b**), 3% rGO-PCL (**c**), 5% rGO-PCL at 1 xK magnification (**d**). (**e**) Expression profile of extracellular matrix and adhesion molecules in HMSCs maintained on rGO-PCL surfaces for 7 days. Heat map reporting under expressed (green) and overexpressed (red) genes in 1.6% rGO-PCL (Group 1), 3% rGO-PCL (Group 2), and 5% rGO-PCL (Group 3) compared with pure PCL (Control Group).
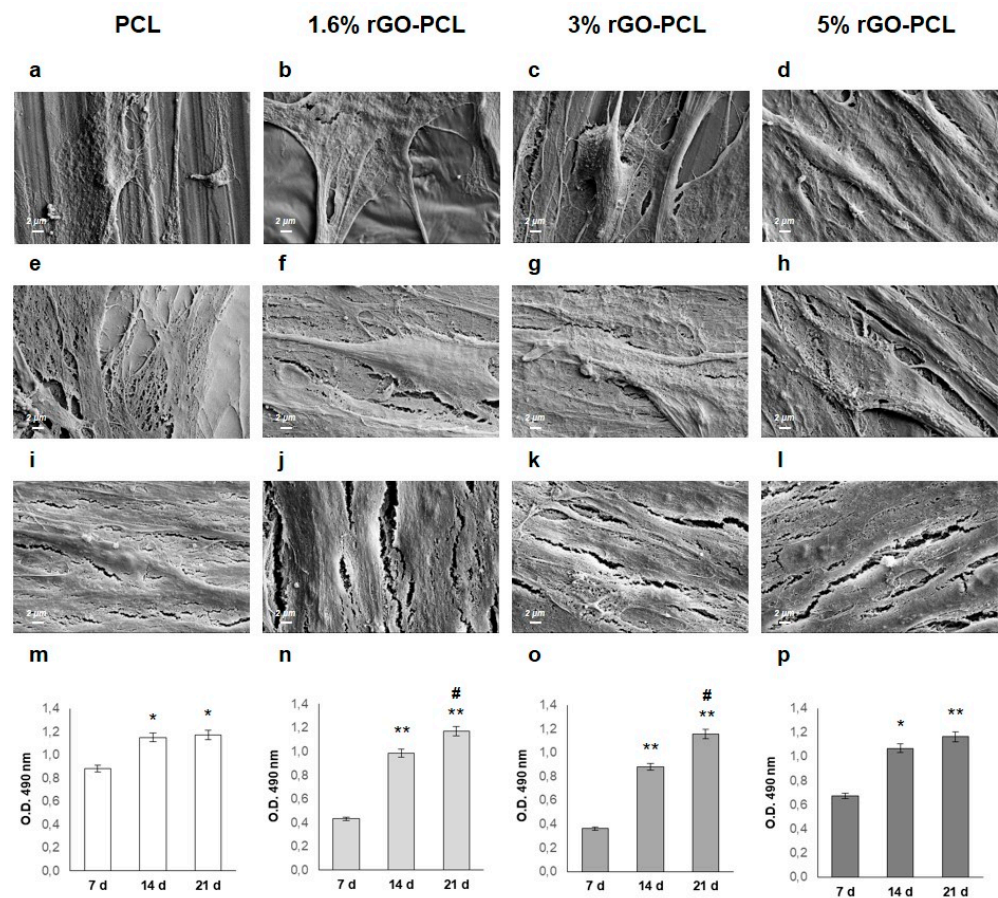
3.4. Osteogenic Differentiation of Stem Cell on rGO-PCL Surfaces

In order to investigate rGO-PCL surfaces as promising platform for osteogenic differentiation, cultures of HMSCs were monitored up to 21 days. Firstly, the adhesion and proliferation of HMSCs were evaluated by microscope and enzymatic analyses (Figure 4). As shown by SEM images at 7 days, HMSCs were able to adhere to surfaces of rGO-PCL samples by numerous filopodia (Figure 4a–d). After 14 days of culture, HMSCs appeared more spread out, and an increased cell coverage on each rGO-PCL surface was observed (Figure 4e–h). After 21 day of culture, the number of HMSCs attached to the surfaces was indistinguishable, which implied that the cells were evenly distributed on rGO-PCL surfaces (Figure 4i–l). These observations were in agreement with MTS assay results (Figure 4m–p). In general, the magnitude of the MTS reduction provides information on the number of viable cells indicating if materials support the adhesion and proliferation of the cells. Compared with 7 days of culture, cell proliferation showed a significant increase at the 14th ($p < 0.05$ for PCL and 5% rGO-PCL, $p < 0.01$ for 1.6 %rGO-PCL and 3% rGO-PCL) and 21st day ($p < 0.05$ for PCL, $p < 0.01$ for 1.6 %rGO-PCL, 3% rGO-PCL and 5% rGO-PCL). Furthermore, cell proliferation exhibited a significant increase ($p < 0.05$) on 1.6% rGO-PCL and 3% rGO-PCL by comparing 21 days of culture with 14 days.
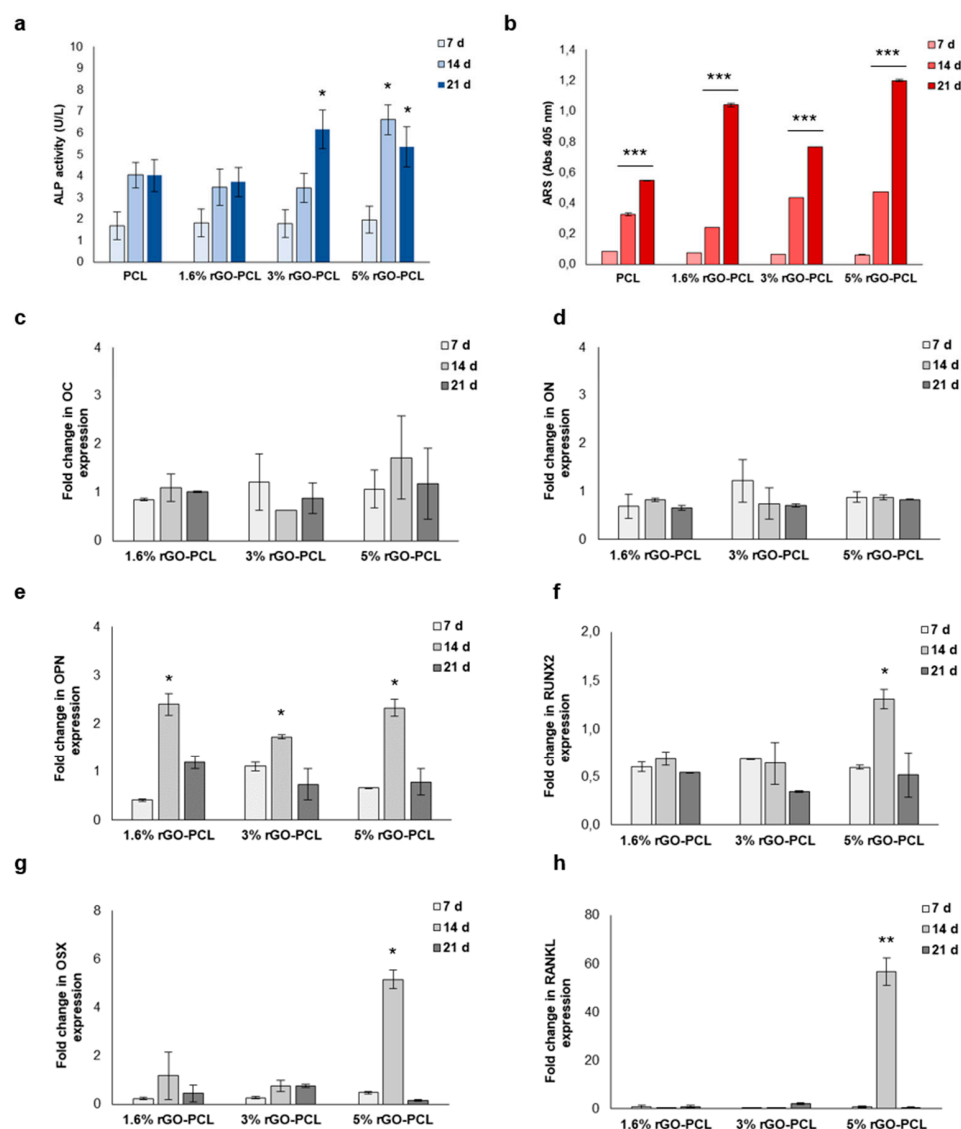
The differentiation of HMSCs towards osteoblast phenotype on rGO-PCL surfaces was investigated by the quantification of ALP activity and mineral matrix deposition, and by gene expression profile of osteogenic markers (Figure 5). Compared to 7 days of culture, ALP activity was increased at 14 days. Nevertheless, a significant ($p < 0.05$) increase was observe only in HMSCs seeded on 5% rGO-PCL. At 21 days, ALP activity remained stable on 1.6% rGO-PCL as well as on PCL, and significantly ($p < 0.05$) increased on 3% rGO-PCL. On 5% rGO-PCL, ALP activity at 21 day is less compared to 14 day, but significantly ($p < 0.05$) greater than 7 days (Figure 5a). The Alizarin Red S (ARS) quantification performed on rGO-PCL samples confirmed the progression of osteogenic differentiation up to 21 days. In particular, the matrix deposition was significantly ($p < 0.001$) boosted at 14 and 21 days, and largely on 5% rGO-PCL surface (Figure 5b). In addition, gene expression for both early

and late osteogenic differentiation markers osteocalcin (OC), osteonectin (ON), osteopontin (OPN), runt-related transcription factor 2 (RUNX2), osterix (OSX), and receptor activator of NF-kB ligand (RANKL) was assessed (Figure 5c–h). The mRNA expression of the osteogenic markers on each rGO-PCL surface was compared with that on PCL at each time point. The comparison shown that on rGO-PCL the gene expression of matrix proteins OC and ON is similar to those on PCL. Further, 1.6% rGO-PCL, 3% rGO-PCL, and 5% rGO-PCL showed significantly ($p < 0.05$) enhanced mRNA expression level of OPN, which were 2.4 ± 0.22, 1.7 ± 0.04, and 2.3 ± 0.17 fold higher than the PCL group at 14 days, respectively. The transcription factors RUNX2 and OSX were significantly ($p < 0.05$) up regulated on 5% rGO-PCL at 14 days with a fold change of 1.3 ± 0.2 and 5.1 ± 0.4, respectively. In addition, a significant ($p < 0.01$) upregulation of RANKL is also observed on 5% rGO-PCL compared to control condition.

Figure 4. Adhesion and proliferation of HMSCs on rGO-PCL surfaces in osteogenic differentiation medium. SEM images (5 ox magnification) after 7 (**a**–**d**), 14 (**e**–**h**), and 21 days (**i**–**l**) of culture. MTS assay at 7, 14, and 21 day (**m**–**p**). Data are expressed as mean $\pm$ SD. Multi comparison statistical analysis were performed by using one-way ANOVA. T test was to perform all pairwise comparisons between group means. Note: * $p < 0.05$ and ** $p < 0.01$ mark significant changes compared to 7 days of culture. # $p < 0.05$ marks significant changes compared to 14 days of culture.

Figure 5. Differentiation of HMSCs towards osteoblast phenotype on rGO-PCL scaffolds up to 21 days. ALP activity (**a**). Quantification of mineral matrix deposition (**b**). Gene expression profile of osteogenic markers: osteocalcin (**c**), osteonectin (**d**), osteopontin (**e**), runt-related transcription factor 2 (**f**), osterix (**g**), receptor activator of NF-kB ligand (**h**). Data are expressed as mean ± SD. Multi comparison statistical analysis were performed by using one-way ANOVA. T test was to perform all pairwise comparisons between group means. Note: * $p < 0.05$, ** $p < 0.01$ and *** $p < 0.001$ mark significant changes compared to pure PCL at each time point.

4. Discussion

Different rGO-PCL compounds were manufactured through the fine dispersion of low percentage of rGO powder in molten PCL. The most suitable combinations to obtain a better dispersion of rGO in molten PCL was obtained with a filler content less than 5% by weight. The 1.6%rGO-PCL, 3%rGO-PCL, and 5%rGO-PCL composites were prepared through extrusion process followed by injection molding. Chemical analysis demonstrated the effective incorporation of rGO into the PLC matrix. The Raman spectra of the composites shown typical characteristics of both PCL and rGO [19,22]. In 1.6% rGO-PCL, the peculiar peaks and bands of PCL and rGO were present, whereas in 3% rGO-PCL and 5%rGO-PCL the bands of rGO were dominant.

After sterilization, antibacterial activity and biocompatibility of rGO-PCL compounds were investigated. By various approaches, the antibacterial activity of each compound on

Gram-negative and Gram-positive bacteria was analyzed. The bacteriostatic properties against Gram-positive bacteria were rGO dose-dependent, and 5% rGO-PCL compound was the best in the prevention of *S. aureus* and *S. pyogenes* growth. Instead, no bacteriostatic effect was shown towards the Gram-negative bacteria *E. coli* and P. aeruginosa. Although a reduction in *E. coli* adhesion was detected as the rGO percentage increases, a minor reduction in pyocyanin production in *P. aeruginosa* was observed. All compounds were biocompatible as demonstrate by incubation in direct contact with cultures of murine fibroblasts for 48h. Our results shown cell viability between 81% and 90% for rGO-PCL compounds. According to in vitro cytotoxicity standard, a percentage reduction in viability greater than 30% compared to the control is to be considered a cytotoxic effect [14]. Thus, the rGO-PCL compounds exhibited no cytotoxicity, confirming that rGO-PCL, as pure PCL, has potential biomedical applications.

The adhesion and migration of stem cells were investigated by microscopy and molecular analyses. Stem cells exhibited flat morphology on tested surfaces. Cell physiological processes including growth, division, differentiation, and migration are affected by the adhesion to extracellular components. Via adhesion molecules, cells bind themselves to ECM substratum defining tissue shape, structure, and function. The cell–matrix and cell–cell interactions on rGO-PCL surfaces were also investigated by gene expression profile. In particular, basement membrane constituents, collagens, integrins, selectins, catenins, cell-adhesion molecule family members, and metalloproteinases (MMPs) as well as their inhibitors were analyzed. Twenty-five percent of the genes investigated showed up- or down-regulation compared to pure PCL; the remaining genes conversely were equally expressed. Among the rGO-PCL formulations tested, the one with the highest percentage of rGO resulted in high-level expression of integrins, catenins, and other proteins of ECM. Integrins are heterodimeric proteins composed of alpha and beta subunits that function as transmembrane linkers between the ECM and the actin cytoskeleton of cells. It is known that the chemistry of the substrate can affect both the types of protein adsorbed onto the surface and the conformation of self-same proteins. This in turn induces changes in integrin expression on cell surface [24]. Integrins bind laminins, glycoproteins composed of three different subunits (α-chain, β-chain, and γ-chain) combined and expressed in at least 16 different isoforms in human. By binding cell-surface receptors, laminins regulate vital cellular responses, such as phenotype maintenance, migration, proliferation, and differentiation [25]. Catenins are cell-adhesion molecules that fine control HMSC functions by the intensity of Wnt/β-catenin signals. For instance, proliferation and self-renewal of HMSCs were promoted only under low levels of Wnt/β-catenin, whereas osteogenic differentiation was promoted in a manner proportional to the intensity of the Wnt signals. Therefore, β-catenin functions as a distinct transactivation molecule depending on its level of accumulation to induce different transcriptomic changes in the HMSCs [26]. Moreover, the expression of CD44 gene was rGO dependent. The CD44 protein binds various components of ECM, such as hyaluronan, and through these interactions, it influences cellular behavior, adhesion, and migration. In addition, CD44 proteins functions as specialized platform for growth factors and MMPs. Precisely, the binding CD44-hyaluronan triggers cell migration; instead, the cleavage of CD44 by MMPs hinders migration [27]. The MMPs are key factors of ECM remodeling, the essential prerequisite for the early stages of cell adhesion on biomaterials [28]. Among the MMPs investigated, the MMP11 and the inhibitor TIMP1 were upregulated on all rGO-PCL surfaces. Moreover, on the rGO-PCL surfaces the homeostasis of ECM is favored through the up-regulation of the transmembrane molecule SGCE, that regulates cell-matrix adhesion, and the up-regulation of ECM1 that organizes a variety of extracellular and structural proteins of ECM. The mechanical properties and the expression profile of HMSCs maintained on rGO-PCL surfaces seem to be influenced by the amount of rGO into PCL matrix. In particular, cells maintained on 5% rGO-PCL for 7 days show a gene expression profile for adhesion molecules and extracellular proteins referable to the early stages of osteogenic differentiation. Based on these findings, rGO-PCL surfaces were valued as substrates for the osteogenic differentiation of HMSCs. By microscopy and enzymatic

analyses, cell adhesion and proliferation were monitored over three weeks. After 21 day of culture, cells were metabolically active and broadly distributed on rGO-PCL surfaces. However, differences in gene expression profile, in ALP activity, and in mineral matrix deposition were observed between the rGO-PCL surfaces. Generally, ALP is considered an early marker of osteoblast differentiation. As ALP is a byproduct of osteoblast activity, increased level of ALP refers to active bone formation. Conversely, the calcium deposition in matrix is considered a late marker for osteogenesis as matrix mineralization begins after the initial accumulation of osteoblast proteins, such as ALP [29]. Among the tested combinations, only 5% rGO-PCL compound showed maximum ALP activity at 14 days followed by maximum mineralized matrix deposition at 21 days. Furthermore, the expression of the main genes involved in osteogenic differentiation, including OC, ON, OPN, OSX, RUNX2, and RANKL gene was investigated. The gene expression of OC and ON did not change over time in any of the conditions tested. Conversely, OPN gene expression is significantly improved on all surfaces. Instead, the expression of RUNX2, OSX, and RANKL merely increased on 5% rGO-PCL surface. OC, ON, and OPN are major non-collagenous proteins secreted by osteoblasts and pre-osteoblast. They are involved in bone matrix deposition and organization [30]. RUNX2 is the major transcription factor necessary for osteoblast differentiation, as it regulates many bone-related genes. OSX is another osteoblast-specific transcription factor downstream gene of RUNX2 involved in the osteoblast differentiation pathway [31]. RANKL is produced and secreted by osteoblasts during the late stage of differentiation [32–40]. Morphological, mechanical, and gene expression results indicate that the osteogenic differentiation of stem cells is improved on rGO-PCL surfaces in rGO dose-dependent manner. Although cell proliferation and migration are similar on all scaffolds, merely 5% rGO-PCL surface shown ALP activity, mineral matrix deposition, and RUNX2, OSX, OPN, and RANKL gene expression compatible with an effective osteogenic differentiation.

5. Conclusions

In conclusion, this study demonstrated the perfect suitability of rGO-PCL for the adhesion, proliferation, migration, and osteogenic differentiation of HMSCs. Firstly, PCL-based compounds with 1.6%, 3%, and 5% rGO were manufactured by extrusion. After sterilization, the biocompatibility of all compounds was demonstrated by measuring the cell viability according to the international standard for medical devices. Surprisingly, rGO-PCL compounds showed bacteriostatic properties to Gram-positive bacteria in rGO-dependent manner. The percentage of rGO also regulated the adhesion, morphology and differentiation of the stem cells. The 5% rGO-PCL surface supported the growth of cells and implemented the expression of the ECM components necessary to anchor the cells to itself. Furthermore, it promoted the osteogenic differentiation by ensuring the activity of alkaline phosphatase, the deposition of the mineral matrix, and the expression of proteins crucial for the differentiation in osteoblasts. These results suggest that 5% rGO-PCL has useful properties for bone tissue engineering purposes.

Author Contributions: Conceptualization, B.Z. and L.F.; methodology, M.S. and L.F.; validation, L.F. and F.R.; formal analysis, C.G.; investigation, F.Z. and E.B.; data curation, L.F., C.G., F.R., E.B. and F.Z.; writing—original draft preparation, L.F. and F.R.; writing—review and editing, L.F.; visualization, B.Z.; supervision, B.Z. and P.R.; project administration, B.Z. All authors have read and agreed to the published version of the manuscript.

Institutional Review Board Statement: Not applicable.

Informed Consent Statement: Not applicable.

Data Availability Statement: Not applicable.

References

1. Liu, L.-N.; Zhang, X.-H.; Liu, H.-H.; Li, K.-H.; Wu, Q.-H.; Liu, Y.; Luo, E. Osteogenesis Differences Around Titanium Implant and in Bone Defect Between Jaw Bones and Long Bones. *J. Craniofacial Surg.* **2020**, *31*, 2193–2198. [CrossRef] [PubMed]
2. Javed, F.; Ahmed, H.B.; Crespi, R.; Romanos, G.E. Role of primary stability for successful osseointegration of dental implants: Factors of influence and evaluation. *Interv. Med. Appl. Sci.* **2013**, *5*, 162–167. [CrossRef] [PubMed]
3. Xie, Y.; Li, S.; Zhang, T.; Wang, C.; Cai, X. Titanium mesh for bone augmentation in oral implantology: Current application and progress. *Int. J. Oral Sci.* **2020**, *12*, 37. [CrossRef] [PubMed]
4. Yasin, M.; Tighe, B. Polymers for biodegradable medical devices: VIII. Hydroxybutyrate-hydroxyvalerate copolymers: Physical and degradative properties of blends with polycaprolactone. *Biomaterials* **1992**, *13*, 9–16. [CrossRef]
5. Prabha, R.D.; Kraft, D.C.E.; Harkness, L.; Melsen, B.; Varma, H.; Nair, P.D.; Kjems, J.; Kassem, M. Bioactive nano-fibrous scaffold for vascularized craniofacial bone regeneration. *J. Tissue Eng. Regen. Med.* **2017**, *12*, e1537–e1548. [CrossRef]
6. Kim, S.E.; Yun, Y.-P.; Shim, K.-S.; Kim, H.J.; Park, K.; Song, H.-R. 3D printed alendronate-releasing poly(caprolactone) porous scaffolds enhance osteogenic differentiation and bone formation in rat tibial defects. *Biomed. Mater.* **2016**, *11*, 055005. [CrossRef]
7. Duan, T.; Xu, H.; Tang, Y.; Jin, J.; Wang, Z. Effect of epitaxial crystallization on the structural evolution of PCL/RGO nanocomposites during stretching by in-situ synchrotron radiation. *Polymer* **2018**, *159*, 106–115. [CrossRef]
8. Miao, W.; Wu, F.; Zhou, S.; Yao, G.; Li, Y.; Wang, Z. Epitaxial Crystallization of Poly(ε-caprolactone) on Reduced Graphene Oxide at a Low Shear Rate by In Situ SAXS/WAXD Methods. *ACS Omega* **2020**, *5*, 31535–31542. [CrossRef]
9. Babaie, A.; Rezaei, M.; Sofla, R.L.M. Investigation of the effects of polycaprolactone molecular weight and graphene content on crystallinity, mechanical properties and shape memory behavior of polyurethane/graphene nanocomposites. *J. Mech. Behav. Biomed. Mater.* **2019**, *96*, 53–68. [CrossRef]
10. Damonte, G.; Vallin, A.; Fina, A.; Monticelli, O. On the Development of an Effective Method to Produce Conductive PCL Film. *Nanomaterials* **2021**, *11*, 1385. [CrossRef]
11. Spradling, A.C.; Drummond-Barbosa, D.; Kai, T. Stem cells find their niche. *Nature* **2001**, *414*, 98–104. [CrossRef] [PubMed]
12. Naqvi, S.M.; McNamara, L.M. Stem Cell Mechanobiology and the Role of Biomaterials in Governing Mechanotransduction and Matrix Production for Tissue Regeneration. *Front. Bioeng. Biotechnol.* **2020**, *8*, 597661. [CrossRef] [PubMed]
13. Gardin, C.; Ricci, S.; Ferroni, L.; Guazzo, R.; Sbricoli, L.; De Benedictis, G.; Finotti, L.; Isola, M.; Bressan, E.; Zavan, B. Decellularization and Delipidation Protocols of Bovine Bone and Pericardium for Bone Grafting and Guided Bone Regeneration Procedures. *PLoS ONE* **2015**, *10*, e0132344. [CrossRef] [PubMed]
14. Pankongadisak, P.; Suwantong, O. Enhanced properties of injectable chitosan-based thermogelling hydrogels by silk fibroin and longan seed extract for bone tissue engineering. *Int. J. Biol. Macromol.* **2019**, *138*, 412–424. [CrossRef]
15. Ferroni, L.; Tocco, I.; De Pieri, A.; Menarin, M.; Fermi, E.; Piattelli, A.; Gardin, C.; Zavan, B. Pulsed magnetic therapy increases osteogenic differentiation of mesenchymal stem cells only if they are pre-committed. *Life Sci.* **2016**, *152*, 44–51. [CrossRef] [PubMed]
16. Gardin, C.; Ferroni, L.; Erdoğan, Y.K.; Zanotti, F.; De Francesco, F.; Trentini, M.; Brunello, G.; Ercan, B.; Zavan, B. Nanostructured Modifications of Titanium Surfaces Improve Vascular Regenerative Properties of Exosomes Derived from Mesenchymal Stem Cells: Preliminary In Vitro Results. *Nanomaterials* **2021**, *11*, 3452. [CrossRef]
17. Cecchinato, F.; Karlsson, J.; Ferroni, L.; Gardin, C.; Galli, S.; Wennerberg, A.; Zavan, B.; Andersson, M.; Jimbo, R. Osteogenic potential of human adipose-derived stromal cells on 3-dimensional mesoporous TiO2 coating with magnesium impregnation. *Mater. Sci. Eng. C* **2015**, *52*, 225–234. [CrossRef]
18. Pfaffl, M.W. A new mathematical model for relative quantification in real-time RT-PCR. *Nucleic Acids Res.* **2001**, *29*, e45. [CrossRef]
19. Wesełucha-Birczyńska, A.; Świętek, M.; Sołtysiak, E.; Galiński, P.; Płachta, L.; Piekara, K.; Błażewicz, M. Raman spectroscopy and the material study of nanocomposite membranes from poly(ε-caprolactone) with biocompatibility testing in osteoblast-like cells. *Analyst* **2015**, *140*, 2311–2320. [CrossRef]
20. Baranowska-Korczyc, A.; Warowicka, A.; Jasiurkowska-Delaporte, M.; Grześkowiak, B.; Jarek, M.; Maciejewska, B.M.; Jurga-Stopa, J.; Jurga, S. Antimicrobial electrospun poly(ε-caprolactone) scaffolds for gingival fibroblast growth. *RSC Adv.* **2016**, *6*, 19647–19656. [CrossRef]
21. Vijayavenkataraman, S.; Kannan, S.; Cao, T.; Fuh, J.Y.H.; Sriram, G.; Lu, W.F. 3D-Printed PCL/PPy Conductive Scaffolds as Three-Dimensional Porous Nerve Guide Conduits (NGCs) for Peripheral Nerve Injury Repair. *Front. Bioeng. Biotechnol.* **2019**, *7*, 266. [CrossRef] [PubMed]
22. Wu, J.-B.; Lin, M.-L.; Cong, X.; Liu, H.-N.; Tan, P.-H. Raman spectroscopy of graphene-based materials and its applications in related devices. *Chem. Soc. Rev.* **2018**, *47*, 1822–1873. [CrossRef] [PubMed]
23. Muzyka, R.; Drewniak, S.; Pustelny, T.; Chrubasik, M.; Gryglewicz, G. Characterization of Graphite Oxide and Reduced Graphene Oxide Obtained from Different Graphite Precursors and Oxidized by Different Methods Using Raman Spectroscopy. *Materials* **2018**, *11*, 1050. [CrossRef]
24. Olivares-Navarrete, R.; Rodil, S.E.; Hyzy, S.L.; Dunn, G.R.; Almaguer-Flores, A.; Schwartz, Z.; Boyan, B.D. Role of integrin subunits in mesenchymal stem cell differentiation and osteoblast maturation on graphitic carbon-coated microstructured surfaces. *Biomaterials* **2015**, *51*, 69–79. [CrossRef] [PubMed]
25. Hagbard, L.; Cameron, K.; August, P.; Penton, C.; Parmar, M.; Hay, D.C.; Kallur, T. Developing defined substrates for stem cell culture and differentiation. *Philos. Trans. R. Soc. B Biol. Sci.* **2018**, *373*, 20170230. [CrossRef] [PubMed]

26. Kim, J.-A.; Choi, H.-K.; Kim, T.-M.; Leem, S.-H.; Oh, I.-H. Regulation of mesenchymal stromal cells through fine tuning of canonical Wnt signaling. *Stem Cell Res.* **2015**, *14*, 356–368. [CrossRef]

27. Ponta, H.; Sherman, L.S.; Herrlich, P.A. CD44: From adhesion molecules to signalling regulators. *Nat. Rev. Mol. Cell Biol.* **2003**, *4*, 33–45. [CrossRef]

28. Albano, C.S.; Gomes, A.M.; Feltran, G.D.S.; Fernandes, C.J.D.C.; Trino, L.D.; Zambuzzi, W.F.; Lisboa-Filho, P.N. Bisphosphonate-based surface biofunctionalization improves titanium biocompatibility. *J. Mater. Sci. Mater. Med.* **2020**, *31*, 109. [CrossRef]

29. Lee, J.-M.; Kim, M.-G.; Byun, J.-H.; Kim, G.-C.; Ro, J.-H.; Hwang, D.-S.; Choi, B.-B.; Park, G.-C.; Kim, U.-K. The effect of biomechanical stimulation on osteoblast differentiation of human jaw periosteum-derived stem cells. *Maxillofac. Plast. Reconstr. Surg.* **2017**, *39*, 7. [CrossRef]

30. Bailey, S.; Karsenty, G.; Gundberg, C.; Vashishth, D. Osteocalcin and osteopontin influence bone morphology and mechanical properties. *Ann. N. Y. Acad. Sci.* **2017**, *1409*, 79–84. [CrossRef]

31. Chen, S.; Gluhak-Heinrich, J.; Wang, Y.; Wu, Y.; Chuang, H.H.; Chen, L.; Yuan, G.; Dong, J.; Gay, I.; MacDougall, M. *Runx2, Osx*, and *Dspp* in Tooth Development. *J. Dent. Res.* **2009**, *88*, 904–909. [CrossRef] [PubMed]

32. Tobeiha, M.; Moghadasian, M.H.; Amin, N.; Jafarnejad, S. RANKL/RANK/OPG Pathway: A Mechanism Involved in Exercise-Induced Bone Remodeling. *BioMed Res. Int.* **2020**, *2020*, 6910312. [CrossRef] [PubMed]

33. Brun, P.; Cortivo, R.; Zavan, B.; Vecchiato, N.; Abatangelo, G. In vitro reconstructed tissues on hyaluronan-based temporary scaffolding. *J. Mater Sci. Mater Med.* **1999**, *10*, 683–688. [CrossRef]

34. Figallo, E.; Flaibani, M.; Zavan, B.; Abatangelo, G.; Elvassore, N. Micropatterned Biopolymer 3D Scaffold for Static and Dynamic Culture of Human Fibroblasts. *Biotechnol. Prog.* **2007**, *23*, 210–216. [CrossRef]

35. Gardin, C.; Bressan, E.; Ferroni, L.; Nalesso, E.; Vindigni, V.; Stellini, E.; Pinton, P.; Sivolella, S.; Zavan, B. In vitro concurrent endothelial and osteogenic commitment of adipose-derived stem cells and their genomical analyses through comparative genomic hybridization array: Novel strategies to increase the successful engraftment of tissue-engineered bone grafts. *Stem Cells Dev.* **2012**, *5*, 767–777. [CrossRef]

36. Azzena, B.; Mazzoleni, F.; Abatangelo, G.; Zavan, B.; Vindigni, V. Autologous platelet-rich plasma as an adipocyte in vivo delivery system: Case report. *Aesthetic Plast Surg.* **2008**, 155–158. [CrossRef] [PubMed]

37. Ettorre, V.; De Marco, P.; Zara, S.; Perrotti, V.; Scarano, A.; Di Crescenzo, A.; Petrini, M.; Hadad, C.; Bosco, D.; Zavan, B.; et al. In vitro and in vivo characterization of graphene oxide coated porcine bone granules. *Carbon* **2016**, *103*, 291–298. [CrossRef]

38. Joshian, K.M.; Shelar, A.; Kasabe, U.; Nikam, L.K.; Pawar, R.A.; Sangshetti, J.; Kale, B.B.; Singh, A.V.; Patil, R.; Chaskar, M.G. Biofilm inhibition in *Candida albicans* with biogenic hierarchical zinc-oxide nanoparticles. *Mater Sci. Eng. C Mater Biol. Appl.* **2021**, *134*, 35527134.

39. Zhang, Y.; Cui, K.; Fu, T.; Wang, J.; Shen, F.; Zhang, X.; Yu, L. Formation of MoSi2 and Si/MoSi2 coatings on TZM (Mo–0.5Ti–0.1Zr–0.02C) alloy by hot dip silicon-plating method. *Ceram. Int.* **2021**, *47*, 23053–23065. [CrossRef]

40. Maharjan, R.S.; Singh, A.V.; Hanif, J.; Rosenkranz, D.; Haidar, R.; Shelar, A.; Singh, S.P.; Dey, A.; Patil, R.; Zamboni, P.; et al. Investigation of the Associations between a Nanomaterial's Microrheology and Toxicology. *ACS Omega* **2022**, *7*, 13985–13997. [CrossRef]